Field Thermal Infrared Imaging Experiments

K. J. Bland
A. R. Gillespie
Geologic Remote Sensing Department,
University of Washington

A. B. Kahle
Jet Propulsion Laboratory, California Institute of Technology,
Pasadena, California

Day/night radiant temperature differences acquired from thermal imaging techniques proved effective in separating four seral stage and one deciduous forest class. Short- and long-term temperature variability of the forest was determined throughout the diurnal cycle, using portable thermal infrared imaging systems. Maximum diurnal temperature differences for each class were calculated and described using Effective Thermal Inertia (ETI) ($a/\Delta T$), developed in this study. Differences in ΔT, and hence ETI, between forest classes are apparently caused by systematic differences in canopy structure. Assuming a uniform albedo, deciduous trees had lower ETI values than coniferous trees, which allowed distinction between the two. ETI values developed from field studies allowed for classification of Thermal Infrared Mutispectral Scanner (TIMS) data.

Introduction

Thermal imaging capabilities in remote sensing have been developed and tested largely from aircraft or satellite, with the result that little attention has been paid to large-scale images that portray temperatures or thermal emissivities at the scales most pertinent to the components and processes in the scene under study. For example, temperatures in a tree are controlled at the leaf level; 1 km^2 pixels can only portray average properties of populations of trees. We can only surmise what goes on at the leaf scale, or make point measurements with thermocouples or radiometers. Recent advances in hand-held imaging systems allow field measurements of temperature images that portray data at the critical large scales. This paper presents the results of a study in which field images were used to study temperatures in stands of trees.

Heightened awareness of timber depletion, the hydrological impact of present logging methods, and endangerment of animal habitat has increased demand for seral stage and forest community mapping by ecologists, timber companies, and conservationists. The geographical extent of the Earth's forest, and the scope and rapidity of the changes in them, make it difficult to do cost-effective field mapping. Currently, aerial photography is widely used as a basis of photo interpretive mapping because in aerial survey it is possible to map entire drainages quickly. However, recent advances in remote-sensing techniques have made it possible to make even larger surveys at frequent intervals in a wide range of spectral regions. New image analysis techniques hold the

potential for improved mapping resolution and accuracy, with only local ground-truthing sites. In particular, advanced thermal infrared sensors make it possible to do detailed temperature studies of the forest. Forest community and seral stage mapping may be enhanced by basing classifications on diurnal forest temperature changes as well as visible wavelength spectral differences.

Previous studies have explored forest mapping using multispectral or hyperspectral VNIR images as well as radar data. An underlying problem with these VNIR data is classification error due to textural, or subpixel roughness, effects. At the 30m pixel scale typical of remote-sensing images, unresolved subpixel shadows can be addressed using mixing theory, but some ambiguity between large-scale topographic effects and sub-pixel roughness effects is inevitable. Phase-angle changes due to time of day and season can result in color differences unrelated to vegetation type, and which therefore reduces classification accuracy. Differences in subpixel shadowing are the basis for seral stage mapping with VNIR data. Uncertainty arises, however, when it is unclear whether shading is due to topographic effects or differences in canopy structures. Large brightness changes due to poor calibration and/or topographic correction can overwhelm spectral differences in the canopy used for classification. Small spectral features in a forest canopy limit the effectiveness of hyperspectral data for doing forest and seral stage classification.

Radar is not attenuated by clouds and, therefore data can be routinely acquired, especially in tropical rain forests where clear skies are uncommon. However, speckle limits the usefulness of radar images for detailed studies. Radar data respond mainly to canopy structure, scattering by trunks and large branches, and scattering by leaves. Radar is therefore only indirectly sensitive to vegetation types, but quite sensitive to seral stage.

Some investigators have taken another step in forest classification and have studied the relationship between the "Normalized Difference Vegetation Index" (NDVI) and temperature of a forested region. For example, Carlson et al. (1994) showed that a decrease in NDVI directly correlates to an increase in surface temperature. Thermal studies are effective in spotting open-canopy regions due to the large temperature differences between trees and bare soil. Areas where exposed soil was visible due to recent logging show a reduction in amounts of green biomass and NDVI. Trends in NDVI plotted against temperature could assist in seral-stage mapping as clearcuts make the transition from bare soil to closed canopy.

Many forestry-related thermal infrared studies have focused on detecting tree moisture stress, timber yields, fires and inventory of acreage involved, and evapotranspiration rates essential for modeling surface fluxes (Hirsch et al., 1971; Idso et al., 1977; Carlson et al., 1995; Friedl, 1995). Until recently, the usefulness of satellites for data acquisition has been constrained by spatial or radiometric resolution. However, with the development of advanced thermal imaging instruments such as JPL's field-portable Quantum Well Infrared Photometer (QWIP) (Gunapala et al., 1996a,b), commercial imaging cameras, and NASA's airborne Daedalus Thermal Infrared Multispectral Scanner (TIMS) (Palluconi and Meeks, 1985), all of which have high spatial resolution and high radiometric sensitivity, it is now possible to conduct theses studies and, further, to investigate the use of TIR data in detailed seral stage and forest community mapping.

Previous Work

Some mapping studies using thermal infrared measurements have concentrated investigation in arid regions, for example for determination of the relative ages of lava flows on volcanoes (Kahle et al., 1988; Crisp et al., 1990; Wood et al., 1990; Kahle et al., 1995). Emissivity differences on weathered surfaces provide a method of estimating lava flow ages. In other examples, thermal emissivities have been used to identify and map evaporites in playas (Crowley and Hook, 1996); lithologies (Rowan, 1993), and mineralogy alteration (Kahle and Rowan 1980). In the relative weathering studies, weathering products and rock coatings masking the underlying mineralogy were the subject of analysis; in most geologic mapping weathering products or even thin accumulations of wind-blown silt or sand reduced accuracy. Partly to distinguish thinly formed bedrock (e.g. <10cm) from thicker modern deposits, Gillespie and Kahle (1977) inverted thermal inertia models to estimate thermal inertia from day/night temperature differences, together with albedo measurements.

(1) Thermal inertia (cal cm^{-2} $s^{-1/2}$ $°C^{-1}$):

$$P = (K\rho c)^{1/2},$$

where K = thermal conductivity (cal cm^{-1} s^{-1} $°C^{-1}$), ρ= density (g cm^{-3}), and c = specific heat capacity (cal g^{-1} $°C^{-1}$). Thermal inertia describes the resistance of a material to changing its temperature. The thermal inertia is normally highest in dense, quartz-rich rocks and lowest in quartz-poor rocks. A weathered desert landscape having a uniform albedo dictated by thin coating of rock varnish might nevertheless have variable P, controlled by differences in K, ρ, or c of the rock substrate. Thermal inertia is a volume property, and the contrast in the thermal inertia of sand and rock is sufficiently different that thinly buried bedrock is detectable. Even under ideal circumstances, however, thermal inertia can only be used to distinguish sand or alluvium from bedrock; contrast among rock types is typically low. Also, apparent values of P are sensitive to sensible and latent heat transfer across the surface (wind and evaporation), parameters difficult to measure from TIR images alone.

The thermal inertia inversion model of Kahle (1977) was sufficiently sensitive to extraneous factors that a simplified approach, yielding Apparent Thermal Inertia (ATI), was developed by Price et al. (1977).

(2) Apparent thermal inertia (cal $sec^{-1}cm^{-1}$ $°C^{-1}$):

$$\mathrm{ATI} = \frac{NC(1-a)}{(T_{day} - T_{night})}$$

where N is a scaling factor arbitrarily set at 1000 that brings the ATI of most natural materials into the range of 0 to 255, a is the apparent albedo, and C (2.0 cal $min^{-1}cm^{-1}$ $°C^{-1}$) is a constant related to the solar flux. ATI was developed to simplify global thermal inertia studies conducted by the Heat Capacity Mapping Mission (HCMM) (Short and Stuart, 1982). The term "apparent" indicates that only the relative thermal inertias were represented. The simplified ATI eliminates the requirement of measuring bi-directional reflectance, topographic irregularities, material densities, and emissivities, all necessary for the calculation of P. Also, the need for atmospheric correction is reduced. ATI studies were designed to look at geological, not vegetated, surfaces.

Characterization of the thermal response of forests to solar heating was addressed by Luvall and Holbo (1989), who described the short-term temperature change of a forested canopy in terms of a thermal response number (TRN).

(3) Thermal response number ($kJm^{-2}°C^{-1}$):

$$TRN = \frac{\sum_{t2}^{t1}(R_n * \Delta t)}{\Delta T},$$

where R_n (kJm^{-2}) is the total net radiation of the sites between times t_1 and t_2, Δt is time between flights, and T is the spatially averaged mean surface temperature. TRN was intended to be used to map percent ground cover. Temperature differences from one part of the scene to the other due to topographic shading were not accounted for, and the technique was best suitable for regions of low relief.

Luvall and Holbo (1989) found that forested regions had higher TRNs compared to cleared areas due to their higher temperature stability. Latent-heat transfer by evapotranspiration of green vegetation dominates the cooling process in the canopy. Surrounding dry soils are not cooled through evaporation and, therefore, are warmer in the peak heating times of the day. At sundown, heat radiating from the soils to the colder atmosphere cools the surface without the solar flux regenerating heat. Vegetation, however, is warmed by the warm air trapped in the canopy.

One limitation inherent in TRN studies is the requirement of measuring or estimating R_n between overflights to solve the radiative energy balance equation. This is sometimes difficult and in any case, limits geographical coverage or the reliability of the TRN data. Short-term temperature fluctuations due to radiative cooling of the canopy surface between overflight times could skew results.

Methods

The earth's surface temperatures result from the balance of fluxes dictated by the conservation of energy (Figure 1):

(4) Conservation of energy (Wm^{-2}):

$$R_n = H + LE + G,$$

where R_n is the net radiative flux incident on the earth's surface resultant from solar radiation, R_{sun}, sky radiation, R_{sky}, and earth-emitted radiation, R_{earth}, H is the sensible heat flux, LE is the latent heat flux, and G is the ground heat flux (e.g., Price, 1985).

Equation 4 explains the response of a system to incoming radiation. Assuming a scene of uniform R_n, the temperature of the components in the scene will depend on surface emissivities, their sensible, latent, and ground fluxes. Sensible heat of the canopy surface is what is measurable by the thermal infrared sensor; latent heat flux draws heat from the system through evaporation of water vapor, but is not directly measurable. In this case, ground flux will be thought of as constant across the forest. Assuming emissivities of 0.98 (Smith, 1983), temperature differences among trees in a single scene are influenced by varying amounts of latent and sensible heat transfer, which is controlled by varying rates of evaporative cooling, amounts of photosynthetic and non-photosynthetic vegetation, voids in the canopy facilitating aerodynamic sensible and latent heat transfer, and time of day. Seasonal differences are not neglected in this study, but are accounted for by the factors listed above.

Driving trees' nutrient engine is evapotranspiration, which also protects leaves from cell damage due to overheating. Dependent on moisture availability, during periods of maximum heating, evapotranspiration can be the dominate cooling process. Therefore, using thermal inertia (or apparent thermal inertia) to characterize forested regions would not be appropriate due to the latent heat flux component. We propose a simplified method related to both ATI and TRN, but because we

regard day/night ΔT differences among tree types as dominated by exchange of heat from the interior of the canopy to the air, we feel that some analog of thermal inertia is an appropriate, physically based measure for use in forest community mapping. We call this parameter "effective thermal inertia" to distinguish it from P or ATI, a property of solids rather than canopies. The derivation of ETI is discussed and justified below.

(5) *Effective Thermal Inertia (°C):*

$$\mathrm{ETI} = \frac{1-a}{\Delta T_{max}},$$

where ΔT_{max} is the maximum temperature contrast of the canopy surface through one diurnal cycle, and a is its apparent albedo or reflectance. Unlike albedo of a rock or soil which can be measured in the lab, the apparent albedo of a canopy is a combination of factors (shade, leaves, limbs, trunk) which changes with time. ETI is a measure of how different forest types balance the conservation of energy equation. Although part of the ETI equation, for this study apparent albedo is assumed to be constant over the canopy surface. ETI defined this way is essentially $(\Delta T)^{-1}$. This assumption may be largely true for a closed canopy, but is invalid where bare soil is exposed. The simplicity of the ETI equation allows for data collection using single-channel thermal infrared field-portable sensors. There is no requirement for multispectral data such as with ATI studies to determine albedo. Unlike TRN, this method does not require measurements or estimations of net solar radiation.

To study the effectiveness of ETI in forest mapping, three separate experiments were performed using different thermal infrared imaging systems. The first used a thermal scanner from FLIR Systems Inc. (FSI) (Table 1) to measure the variability of a hardwood/coniferous forest at two time scales: 10 seconds and ~10 hours. The second utilized JPL's new QWIP camera (Table 1) to determine the spatial variability of canopy temperatures in a mixed forest. The third used Nasa's airborne Daedalus Thermal Infrared Mutispectral Scanner (TIMS) (Table 1) to apply ETI to forest mapping in a remote-sensing context.

Results of ETI studies

1) Short - and Long-Term Radiant Temperature Variability of a Mixed Canopy

A time-series of thermal infrared images was obtained 15 May 1997 using the University of Washington's field-portable FSI thermal imaging system to inspect a forested hillslope from a nearby ridge. Data were collected every 10 seconds for ~2 ½ diurnal cycles (61 hours). The goal of was to study the short- and long-term spatial temperature variability of a mixed canopy through the diurnal cycle. The study site was in the Mt. Baker-Snoqualmie National Forest, 64 km east of Seattle, Washington and was chosen for its mixed conifer/deciduous canopy and complete canopy closure. The view was towards the south. Six measurement points with 1m spatial averaging were chosen to test the radiant temperature variability among different tree species. Points were chosen on north-facing limbs. Three Douglas firs, two chestnuts, and one madrona tree, all 15-20m in height, were chosen for investigation. Trees were selected that were spaced approximately 30m from one another and were surrounded by other coniferous and deciduous trees. Bare soil or rocks were not visible through the canopy.

Frequent measurement of radiant temperature over nearly three diurnal cycles enabled estimation of the correlation between temperature histories for different tree types at different time scales. This is done to determine at which scale species separation was most

effective; short-term (<10 min) fluctuations in canopy temperatures are associated with wind effects and changes in atmospheric attenuation in solar irradiance where long-term (>1 hr) fluctuations related to temperature changes are associated with diurnal warming and cooling.

Short-term temperature independence from one tree to another is greater than long-term independence. As illustrated in Figure 2a, temperature values drift as much as 3°C/minute on the short-term and are less correlated than long-term fluctuations. This can be explained by aerodynamic sensible heat transfer. The phase differences among the curves are consistent with wind moving across the field of view, from tree to tree.

Figures 2b and 2c show the warming and cooling curves of the three deciduous and the three coniferous trees, respectively throughout nearly three diurnal cycles. The shapes and slopes of the diurnal curves are repeatable and are directly related to tree type and differ mainly with amplitude. The diurnal pattern for the deciduous trees were consistently different than the pattern for the Douglas-firs. Gaps in the temperature histories are when temperatures dropped below the minimum and rose above the maximum dynamic range of the FLIR system.

Figure 2d illustrates the averaged diurnal curves of the coniferous and deciduous trees. A rapid increase in canopy temperature at sunrise (6:30am), followed by a peak in the late afternoon (4:00pm) was characteristic for both tree types. After sunset (8:15pm), without the addition of a solar flux, both tree types rapidly cooled. Tree temperatures steadily decreased to their minimum just prior to the following sunrise.

Although the tree temperatures appeared to follow similar diurnal warming and cooling patterns dictated by radiative flux (R_n) and sensible and latent heat transfer, not all tree types warmed and cooled at the same rates. Shortly after sunrise there was a rapid increase in canopy temperature, and the two different tree types were nearly the same. At around 9:00am the slope for the coniferous tree curve diverged from that for the deciduous tree. The slope of the deciduous trees remained constant while the slope of the coniferous trees decreased.

When solar irradiance was at its peak during the midday (1:00pm) there was an average temperature difference between the two tree types of around 2.5°C. The deciduous trees reached their peak temperature around 1:00pm and remained fairly constant until 5:30pm, just prior to sunset. The coniferous trees continued to warm throughout the entire day until just prior to sundown. It was at sundown when a temperature cross-over point occurred and the deciduous and coniferous trees were the same temperature. The absence of solar heating drove the scene temperatures down, producing negative slopes for all trees. However, the slope of the deciduous curve was, again, steeper than that of the coniferous curve. After 10:00pm the coniferous trees remained approximately 1.5-2°C warmer than the deciduous trees, until around sunrise (8:00am) when the next cross-over point occurred.

Figure 3 is a plot of the temperature difference, produced by subtracting the deciduous trees' temperatures from the coniferous trees', throughout the 61-hour data collection period. The maximum daytime difference, represented by a sharp peak in the curve, occurred around 1:00pm. The maximum nighttime temperature difference, represented by a trough in the curve, occurred around 2:00am. The distinct, but artifactual, gaps that occur in the curve just prior to sunrise and during the peak heat of the day result from the out-of-range temperatures.

2) Spatial Variability of Canopy Temperatures

The purpose of this experiment was to evaluate the radiant temperature variability of a forest canopy during a 24-hour cycle. This was assessed using JPL's QWIP imaging camera. Canopy temperatures in mature or closed canopy forests on clear sunny days are within a few degrees of air temperature (Smith et al., 1981; Kaufman, 1984). The QWIP camera, with its high radiometric sensitivity, is capable of resolving small temperature differences or variations that may exist among different tree species. A diurnal series of images was taken 22 April 1996, using the QWIP camera in the Yolla Bolly National Forest, approximately 70 km SSW of Red Bluff, CA. Due to rainfall the previous evening, the ground and vegetation were damp during the morning hours. There was partial cloud-cover in the morning, but sunny conditions prevailed during daylight hours. Air temperatures hovered around 20°C throughout the warm part of the day. Nighttime air temperatures dropped to around 10°C. The camera was mounted on a hillside overlooking mixed coniferous and deciduous trees that faced north and sloped ~20°. Canopy closure was nearly 100% with minimal bare spots and outcrops. Images were obtained every fifteen minutes and were calibrated to on-site blackbody measurements, assuming an emissivity of 0.99 (Smith, 1983), to determine scene temperatures.

At sunrise radiant temperatures across the scene were uniform. After sunrise, temperatures rose rapidly due to solar heating. As the canopy temperatures increased, areas of uniform temperatures became differentiated, spatially and thermally; these corresponded to shadowed regions (Figure 4a).

Spatial patterns developed as solar irradiance heated the canopy surface. These patterns corresponded to groups of warmer deciduous and cooler coniferous trees. Greatest temperature contrast between coniferous and deciduous trees occurred as solar irradiance peaked near the midday (Figure 4b). The deciduous trees became 2.5-3°C warmer than coniferous trees in the afternoon.

At sundown, scene radiant temperatures began to drop. The deciduous trees, however, systematically lost heat more rapidly than the coniferous trees. Shortly after sundown the temperatures of the coniferous and deciduous trees were the same.

As the two tree types continued to radiate stored heat rapidly to the surroundings, the coniferous canopy remained warmer throughout the night. Approximately 2:00am marked the maximum temperature contrast between the deciduous and coniferous canopies (Figure 4c). The conifers remained 2.0-2.5°C warmer than the deciduous trees until sunrise.

When the morning, mid-day, and nighttime images are registered and combined into one image, a false-color of the time-series ("chronochrome") is produced (Figure 5). The red channel is assigned to the 7:00am image, the green channel to the 2:00pm image, and the blue channel to the 2:00am image. With this one false-color image it is possible to distinguish the coniferous and deciduous tree types with confidence. Since both tree types had the same temperature in the early morning (7:00am) they display equal mounts of red. The deciduous trees appear more yellow (red + green) compared to the coniferous trees due to their higher temperature values in the 2:00pm image. The conifers were cooler than the deciduous trees in the day and warmer at night. Therefore, they appear magenta (red + blue) and cyan (green + blue).

The QWIP imaging camera proved useful in separating coniferous and deciduous trees. Temperature contrast of 4.5-5.5°C between daytime and nighttime images, demonstrated in Figures 4a and 4b, are well within the sensitivity range of today's airborne instruments such as NASA's TIMS. These findings justified further studies using day/night

thermal image pairs of forested regions for community mapping.

3) Forest Community Mapping Using Effective Thermal Inertia

The purpose of this investigation was to test the extendibility of the field-based effective thermal inertia studies to airborne thermal scanners. Bridging the gap between previous effective thermal-inertia field experiments and TIMS data would allow for large-scale forest classification studies. The objective was to produce a land-use map separating different seral stage and forest communities.

A series of TIMS overflights covering the H.J. Andrews Experimental Forest were obtained 5 August 1985 (Holbo and Luvall, 1988). The 6500ha watershed is located in the central-western Cascade Mountain Range, 45 miles east of Eugene, OR. Elevation ranges from about 400 to 1500m (Luvall and Holbo, 1989). The watershed represents the dense coniferous forests of Douglas-fir and western hemlock typical for the western slopes of the Cascade Mountains (Hawk et al., 1978). Forest vegetation ages range from recent clearcuts (<1 year) to old growth Douglas-fir (>450 years)(Sader, 1986). Flight altitude dictated an average spatial resolution of eight meters. The daytime flights (Figure 6a) were flown at 1:37pm local time (PDT), which coincides with maximum solar irradiance. Night flights (Figure 6b) were flown shortly after sundown (9:53pm), when latent and sensible heat flux dominated due to lack of solar radiance. These overflight times were optimum for maximizing ΔT between forest classes as determined by FLIR and QWIP studies.

Atmospheric profiles for temperature, water vapor, and pressure were inferred assuming uniform elevation for a typical mid-latitude, cloudless, late-summer day. The atmospheric profile was used with the LOWTRAN-6 model (Kneizys et al., 1983) to compute atmospheric transmissivity and path radiance. Reflected downwelling sky irradiance was minimal because forest reflectivities are around 1% (Salisbury, 1988). The output from LOWTRAN-6 was later combined with calibrated TIMS data to determine surface land-leaving radiance. Inverting the Planck equation for these values yielded surface temperatures. Co-registration of the day/night image pairs was performed using PICREG, a registration program developed at JPL and the University of Washington. Due to high atmospheric attenuation by H_2O, O_3, and CO_2, TIMS channels 1 (8.2-8.6μm), 4 (9.4-10.2μm), and 6 (11.2-12.2μm) were eliminated from the data set. Temperature values in the remaining channels 2,3, and 5 were averaged to eliminate noise and small perturbations in apparent temperature values between channels.

Once the day/night temperature image pair was calibrated and co-registered a difference image was produced (Figure 7). This image represents the nighttime temperatures subtracted from the daytime. Clearcuts were hot in the day and cold at night, as represented by a positive value in the difference image. Areas that appear dark represent little change in surface temperature from day to night, where bright areas represent areas of large differences. Temperature differences range from a minimum of 0°C for the reservoir in the lower left of the image, to a maximum of 36°C for a recent clearcut in the upper left of the image.

Luvall and Holbo (1989) used TIMS images over the H.J. Andrews Experimental Forest to model surface temperature distributions in forested landscapes. They were able to distinguish three surface types using day/night thermal image pairs: old growth, young plantation, and old regeneration. Using data from their study in conjunction with ETI studies presented earlier, each of the forest

classes investigated were assigned a day/night temperature differences value (Table 2). Each pixel in the image was classified depending on its day/night temperature difference, essentially sorting the image by differences in effective thermal inertia. Areas where bare soil is exposed (e=0.97) have emissivities slightly less than that of vegetation (e = 0.985), but in this study they were assumed to be equal.

The classified image (Figure 8b) produced from the ΔT classification scheme separates each class by its ETI and assigns it a specific color. A 6x6 median filter was applied to the image in attempt to eliminate random scanner noise and misclassification due to misregistration of the day/night images. Assuming forest classes (i.e., clearcuts, forest stands) are no smaller than 8 pixels (40m), misclassification due to filtering is slight. To test the reliability of the classified image, Figure 8b is compared with a seral stage GIS map (Figure 8a), taken from the Long-Term Ecological Research (LTER) archives (Halpern and Spies, 1995). Comparison of the GIS overlay and image show high spatial correlation for clearcut areas. Classification errors along clearcut boundaries are due to misregistration and to temperature mixing within pixels. Mixed boundaries will appear to have a higher ETI than inner pixels. Therefore, an erroneous shift towards older seral stage is indicated.

Discussion

Coniferous trees allow unfiltered sunlight to penetrate deep into the tree structure due to gaps in the canopy. Heating is not limited to the canopy surface, but is distributed into the volume of the tree. Increased amounts of visible shaded regions and distribution of solar energy over a larger area keeps the apparent temperature of the coniferous tree lower than trees with less shadowing and shading. Nighttime temperatures of coniferous canopies are warmer than those of a deciduous canopies. Overlapping of needles and limbs decrease the leaf surface area directly exposed to the sky, hence retarding heat exchange to the atmosphere due to multiple scattering effects. The coniferous canopy essentially insulates itself from the colder atmosphere by inefficiently exchanging heat to the air.

Deciduous trees concentrate leaves along the outside of the tree (Figure 9a). During daylight hours, direct sunlight rapidly warms the horizontally oriented broad leaves along the outer parts of the canopy, allowing little unfiltered light to penetrate into the lower leaves and limbs. The cooling mechanism, evapotranspiration, apparently does not compete with the concentrated heating at the perimeter of the tree. Since voids on the outside of the canopy are few, the shaded regions are not seen by the sensor and the apparent temperature is high. Brutsaert and Sugita (1996) documented that open spaces in the interior of the tree facilitated turbulent transport of latent heat; however, the radiant canopy temperature itself is dominated by solar heating at the surface. Without the input of the solar flux after sundown, deciduous trees lose their stored heat to the colder atmosphere. Due to the concentration of broad leaves out the outer parts of the canopy, heat is lost quickly there.

Given the net solar radiation (R_n, Eqn. 4), canopy structure, microclimates, and amounts of photosynthetic and non-photosynthetic biomass determine the amount of sensible and latent heat flux across the canopy surface. The net radiation is related to canopy temperatures through the Planck equation. Assuming that similar tree species in the same spatial environment have similar latent and sensible heat fluxes, they would have similar canopy temperatures. Conversely, dissimilar species with different canopy structures, microclimates, and amounts of green biomass

would have different canopy temperatures due to different strengths of cooling mechanisms.

By capitalizing on differences in canopy temperature throughout the diurnal cycle, ETI, even with the assumed uniform albedo, has proved useful in differentiating tree types in large-scale images. Using day/night thermal image pairs it is possible to maximize the temperature contrast between forest types and reduce errors due to short-term fluctuations.

ETI studies showed promise in not only differentiating between tree types, but aided in separating forest classes (e.g., seral stage) in small-scale images as well. One advantage in using the thermal infrared spectral region is the high temperature contrast between vegetated and non-vegetated areas. Numerous gray levels separating the two allows for percent ground-cover classes to be defined.

In the H.J. Andrews Forest old-growth areas comprise >90% Douglas-fir trees, when compared to all other elements in the scene, stay cooler during the day and warmer at night. This may be explained by a combination of two phenomena. One, with its high percentage of Douglas-fir, old-growth areas will have a high ETI, as shown in this paper. Two, ancient forests are highly structured at the tree scale which provides a high shade fraction. Therefore, areas of old growth, with complete canopy cover, will have small temperature differences from day to night. Typical ΔT values for old growth are surprisingly low, between 0.1°C and 5°C, suggesting a strong control of temperature by the mature forest.

Areas of old regrowth and closed-canopy deciduous growth, commonly found in riparian zones, fluctuate more in temperature than old growth, but less than areas of partially open canopy. Day/night ΔT values commonly are between 6°C and 10°C.

Two regrowth classes are separated in this study: partially closed and open. As trees are reestablished in a clearcut but is not completely closed, it still may contain low brush and soil visible from above. This will keep ETI values lower than for old-growth canopies. Therefore, diurnal temperature fluctuations will be greater. Day/night ΔT values fall between 10°C and 15°C. Young regrowth areas which are partially open, will have increased amounts of bare soil, low brush, and deciduous vegetation. This will lower ETI values relative to a closed regrowth canopy. Day/night ΔT values range between 15°C and 25°C.

Recent clearcuts exhibit the greatest swings in diurnal temperature. Large amounts of bare soil litter absorb heat during the day with little evaporative cooling or shading/shadowing to lower surface temperatures. At night, sensible heat transfer dominates the heat balance equation (Eqn. 4) and stored heat is radiated back to the cold atmosphere. Recent clearcuts, bare soil, and roads have day/night ΔT values >25°C, but tend not to exceed 36°C.

Misclassification of the image is not limited to mixed boundaries, as discussed earlier. The greatest discrepancy (i.e., with respect to ground truth) in classification occurs in the old-growth class. Many areas of old-growth are misclassified as deciduous/old regrowth. Misclassification, however, tends to be isolated to the lower elevations in the image. This ETI study assumes that radiant tree temperatures are only influenced by there own controlling mechanisms. This, however, is not the case in a natural scene where outside factors exist. One of these factors is phenomena recognized as cold-air ponding. After sundown, cold air will concentrate in the valleys and will cause canopy radiant temperatures to be lower there. This is evident in Figure 6b where a dark streak follows the river valley towards the reservoir in the lower left. In the daytime image (Figure 6a), the same river valley appears warmer than the surrounding forest. This can be explained by multiple scattering in the valleys raising the apparent temperatures there.

Without correcting for cold-air ponding and multiple scattering, higher ΔT and lower ETI values occur in these areas. Areas of old growth are then classified as deciduous/old regrowth.

Conclusions and Future Work

Previous thermal infrared studies have proved effective in determining evapotranspiration rates, modeling land surface fluxes, and estimating clearcut ages. Confidently mapping forest classes with these techniques, however, may prove to be the next attainable achievement. From a practical standpoint, ETI studies are an improvement from previous forest classification studies using thermal infrared for its non-requirement of supporting field data and simplicity of the algorithm. However, ETI studies require maximum thermal contrast between tree types, achievable only by acquiring same day, day/night image pairs. Single polar-orbiting, sun-synchronous satellites take 16-18 days minimum to image the same scene twice. Changes in weather conditions that fluctuate at these time scales make it impractical to use satellite data for these studies. Two satellites 12-hours out of phase is financially unlikely. Although using an airborne platform limits the geographical regions possible for study, it is the best way to acquire thermal data for ETI studies.

Field experiments provide the opportunity to collect long time series of data. When large-scale, airborne studies are performed, however, data collection is often limited to one or two overflights. The use ETI to differentiate tree types requires data acquisition times that optimize temperature contrast in the diurnal cycle. This study demonstrates that maximum temperature contrast occurs around 1:00pm and 2:00am for tree types examined, during these weather conditions, during that time of year. Therefore, a forest community mapping study of a similar area in similar conditions would require data acquisition at these times. Due to the uncorrelated short-term temperature variability within the canopy, however, higher accuracy would be achieved by averaging temperatures measured during several clustered overflights near midnight and early afternoon. Doing so would reduce small-scale temperature differences due to apparently random warming and cooling effects.

The effective thermal inertia, derived from multi-temporal thermal infrared images, appears to be useful for discriminating coniferous from deciduous trees. The inversion is time- and site-specific. Even so, it provides a framework for future forest community mapping studies. Even with limited ground-based measurements, it was found possible to distinguish five different forest types.

Future work using the ETI method might include more detailed studies distinguishing different types of deciduous and coniferous trees and the factors that control their temperatures. Effects due to wind, solar fluctuations, and moisture availability will need to be considered in order to understand the factors involved in attempt to correlate them to canopy temperature. Also, in this study albedo was assumed to be constant among trees, therefore, ETI was strictly dictated by ΔT. Future work could include determining albedo for different tree and surface types to account for slope and azimuth effects on the heating history.

Acknowledgments

We thank Jeff Myers of the NASA AMES Research Center for supplying the TIMS data set, and Sarath Gunapala for access to JPL's QWIP camera. Milton Smith, Gail Yamada, Wen-Hao Li, and Bill Gustafson

assisted in the field and lab. This paper presents aspects of research carried out under contracts NAS 5-31372 and JPL960682, sponsored by the National Aeronautics and Space Administration and the Jet Propulsion Laboratory, California Institute of Technology. The grant from JPL supported the QWIP study, and a gift from the Save the Earth Foundation supported other aspects of the field work.

References

Brutsaert, W., and Sugita, M. (1996), Sensible heat transfer parameterization for surfaces with anisothermal dense vegetation, *Jour. of Atm. Sci.* 53(2):209-216.

Carlson, T. N., Gillies, R. R, and Perry, E.M. (1994), A method to make use of thermal infrared temperature measurements and NDVI to infer surface soil water content and fractional vegetation cover, *Rem. Sens. Rev.* 9(1-2):161-173.

Carlson, T. N., Capehart, W. J., and Gillies, R. R. (1995), A new look at the simplified method for remote sensing of daily evapotranspiration, *Rem. Sens. Environ.* 54:161-167.

Crisp, J., Kahle A. B., and Abbott, E. A. (1990), Thermal infrared spectral character of Hawaiian basaltic glasses, *Jour. of Geophys. Res.* 95(B13):21,657-21,669.

Crowley, J. K., and Hook, S. J. (1996), Mapping playa evaporite minerals and associated sediments in Death Valley, California, with multispectral thermal infrared images, *Jour. of Geophys. Res.* 101(1):643-660.

Friedl, M. A. (1995), Modeling land surface flux using a sparse canopy model and radiometric surface temperature measurements, *Jour. of Geophys. Res.* 100(D12):25,435-25,446.

Gillespie, A. R., and Kahle, A. B. (1977), Construction and interpretation of a digital thermal inertia image, *Photo. Engin. And Rem. Sens.* 43(8): 983-1000

Gunapala, S. D., Liu, J. K., Sundaram, S. V., Shott, C. A., Hoelter, T., Maker, P. D., and Muller, R. E. (1996a), Long wavelength Quantum Well Infrared Photodetector (QWIP) research at Jet Propulsion Laboratory, *SPIE, Orlando, 1996,* 9 pp.

Gunapala, S. D., Liu, J. K., Sundaram, S. V., Shott, C. A., Hoelter, T., Maker, P. D., and Muller, R. E. (1996b), Long-wavelength 256x256 QWIP hand-held camera, *SPIE, Orlando, 1996,* 10 pp.

Halpern, C. B., and Spies, T. A. (1995), Plant species diversity in natural and managed forests of the Pacific Northwest, *Ecolog. Appl.* 5(4): 913-934.

Hawk, G. M., Franklin, J.F., Mckee, W. A., and Brown, R. B. (1978), H.J. Andrews Experimental Forest reference stand system: establishment and use history, *IBP Conif. For. Biome Bull.* No. 12, 79 pp.

Hirsch, S. N., Kruckeberg, R. F., and Madden, F. H. (1971), The bi-spectral forest fire detection system, *Proc. 9th Symp. Rem. Sens. of Environ*, Michigan Inst. of Science and Technology, University of Michigan, Ann Arbor, pp. 2253-2272.

Holbo, H. R., and Luvall, J. C. (1988), Modeling surface temperature distributions in forest landscapes, *Rem. Sens. Environ.* 27:11-24.

Idso, S. B., Jackson, R. D., and Reginato, R. J. (1977), Remote sensing of crop yields, *Science* 189:1012-1013

Kahle, A. B., Abrams, M. J., Abbott, E. A., Mouginis-Mark, P. J., and Realmuto, V. J. (1995), Remote sensing of Mauna Loa, from Mauna Loa Revealed: Structure, Composition, History, and Hazards, *Geophys. Monograph*, pp. 145-169.

Kahle, A. B., Gillespie, A. R., Abbott, E. A., Abrams, M. J., Walker, R. E., Hoover, G., and Lockwood, J. P. (1988), Relative dating of Hawaiian lava flows using multispectral thermal infrared images: a new tool for geologic mapping of young volcanic terranes, *Jour. of Geophys. Res.* 93(B12):15,239-15,251.

Kahle, A. B., and Rowan, L. C. (1980), Mapping of altered and unaltered rock types in the East Tintic Mountains, Utah, *USGS Prof. Paper*, pp. 309.

Kahle, A. B.(1977), A simple model of the Earth's surface for geologic mapping by remote sensing, *Jour. of Geophys. Res.* 82(11):1673-1680.

Kaufman, M. R. (1984), Effects of weather and physiographic conditions on temperature and humidity in subalpine watersheds of the Fraser Experimental Forest, *USDA-Forest Service, Rocky Mtn. For. and Range Exp. Sta. Res. Paper* RM-251, 9 pp.

Kneizys, F. X., Settle, E. P., Gallery, W. O., Chetwynd, J. H., Abreu, L. W., Selby, J. E. A., Fenn, R. W., and McClatchey, R. A. (1983), Atmospheric transmittance/radiance: computer code Lowtran-6, Air Force Geophysics Laboratory Rep. AFGL-TR83-0187, *Optical Phys. Div., Hanscom Air Force Base*, MA 01731, 200 pp.

Luvall, J. C., and Holbo, H. R., and (1989), Measurements of short-term thermal responses of coniferous forest canopies using thermal scanner data, *Rem. Sens. Environ.* 27:1-10.

Palluconi, F. D., and Meeks, G. R. (1985), Thermal Infrared Multispectral Scanner (TIMS): an investigator's guide to TIMS data, *JPL Pub.* 85-32, 14 pp.

Price, J. C. (1985), On the analysis of thermal infrared imagery: the limited utility of apparent thermal inertia, *Rem. Sens. Environ.* 18:59-73.

Price, J. C. (1977), Thermal inertia mapping: A new view of the earth, *Jour. of Geophys. Res.* 82,2582-2590.

Rowan, L. C. (1993), Mapping lithologies in the Iron Hill, Colorado, carbonatite-alkalic igneous rock complex using thermal-infrared multispectral scanner and airborne visible-infrared imaging spectrometer data, *Proceedings of the Thematic Conference on Rem. Sens. for Exploration Geol.* 9; 195-197

Sader, S. A. (1986), Analysis of effective radiant temperatures in a pacific northwest forest using thermal infrared multispectral scanner data, *Rem. Sens. Environ.* 19:105-115.

Salisbury, J. W. (1988), Thermal infrared (2.5 to 13.5 μm)L directional hemispherical reflectance of leaves, *Photogramm. Eng. Rem. Sens.* 54(9):1301.

Short, N. M., and Stuart L. M. (1982), The Heat Capacity Mapping Mission (HCMM)

anthology, *NASA Goddard Space Flight Center,* NASA SP-465, 264 pp.

Smith, J. A., Ranson, K. J., Nguyen, D., and Balick, L. (1981), Thermal vegetation canopy model studies, *Rem. Sens. Environ.* 11:311-326.

Smith, J. A. (1983), Matter-energy interactions in the optical region, in ASP Manual of Remote Sensing, 2nd ed., Falls Church, VA, Chap. 3.

Wood, J. A., Lasserre, M., and Fedosejevs, G. (1990), Analysis of mid-infrared spectral characteristics of rock outcrops and an evaluation of the Kahle model in predicting outcrop thermal inertias, *Rem. Sens. Environ.* 30:169-195.

TABLE 1: Specifications for thermal infrared (TIR) instruments

TABLE 2: Day/night temperature difference forest classification values

FIGURE 1: Energy fluxes at the Earth's surface

FIGURE 2a: Short-term radiant temperature fluctuations of mixed trees

FIGURE 2b: Long-term radiant temperature fluctuations for deciduous trees

FIGURE 2c: Long-term radiant temperature fluctuations for coniferous trees

FIGURE 2d: Averaged long-term radiant temperature fluctuations for coniferous and deciduous trees

FIGURE 3: Deciduous/coniferous radiant temperature differences throughout ~2 ½ diurnal cycles

FIGURE 4: QWIP thermal images of a mixed coniferous/deciduous hillside: a) 7:00am, temperature range = 12 - 20°C, b) 2:00pm, temperature range = 20 - 30 °C, c) 2:00am, temperature range = 10 - 15°C

FIGURE 5: False-color time-series "chronochrome". Red channel = 7:00am, green channel = 2:00pm, blue channel = 2:00am. Coniferous trees appear magenta and cyan where coniferous trees appear green and yellow.

FIGURE 6: H. J. Andrews Experimental Forest TIMS data acquisition, 5 August, 1985: a) daytime radiance, b) nighttime radiance

FIGURE 7: Day/night ΔT image. Old growth had little day/night radiant temperature differences (dark), where clearcuts had large radiant temperature differences (bright). Note: white pixels found in the reservoir are due to out-of-range, saturated pixels.

FIGURE 8: Forest classification using Effective Thermal Inertia (ETI) derived from TIMS data, Willamette National Forest, Oregon. a) GIS ground-truth data, b)ETI classification map

FIGURE 9: Schematic examples of coniferous and deciduous canopy structures showing: a) horizontal orientation of leaves at the periphery of the deciduous tree, and b) layered orientation of limbs in a coniferous tree causing shadowing and allowing light to penetrate into the inner part of the tree.

TABLE 1: Specifications for Thermal Infrared Instruments

Imaging System	Manufacturer	Radiometric Resolution	NEΔT @ 300K	Platform	Image Size (pixels)	Reference
FLIR	FSI (FLIR System, Inc.)	8-12μm (broadband)	0.1-0.2°C	Field-Portable	640x480	N/A
QWIP	JPL (Jet Propulsion Lab.)	9.6μm	~0.05°C	Field-Portable	256x256	Gunapala et al., 1996a,b
TIMS	Daedalus	8.2-12.2μm (6 channels)	0.2-0.3°C	Lear 23 Aircraft	~680x2000	Palluconi and Meeks, 1985

TABLE 2: Day/Night Temperature Difference Forest Classification Values

Forest Class	Day/Night ΔT	ETI Value
Old-Growth	0.0 - 5.0°C	0.0 - 0.2
Deciduous Trees/Old Regrowth	5.1 - 10°C	0.196 - 0.1
Partially Closed Regrowth	10.1 - 15°C	0.099 - 0.067
Open Regrowth	15.1 - 25°C	0.066 - 0.04
Recent Clearcuts	> 25°C	> 0.04

FIGURE 1: Energy fluxes at the earth's surface (conservation of energy)

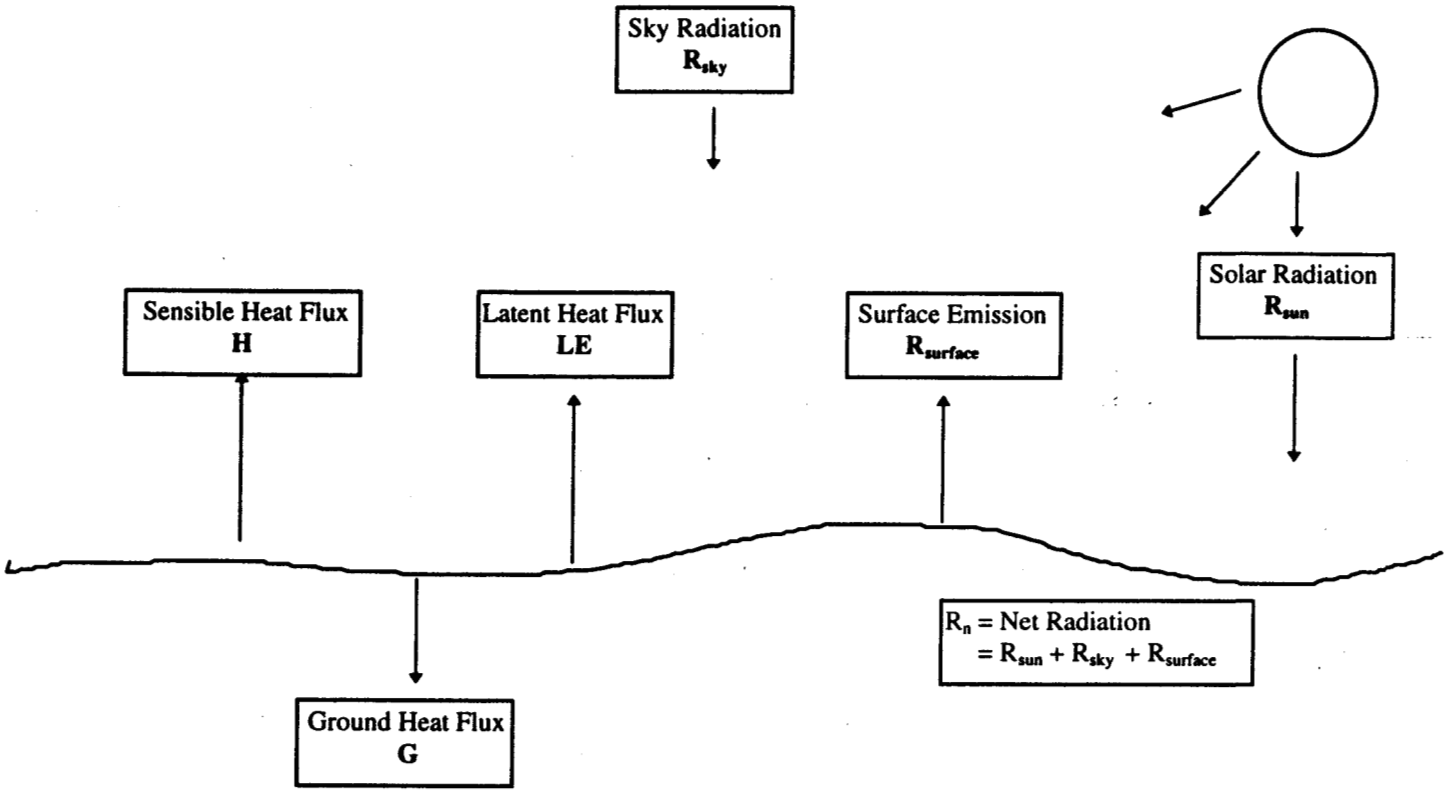

Figure 2a

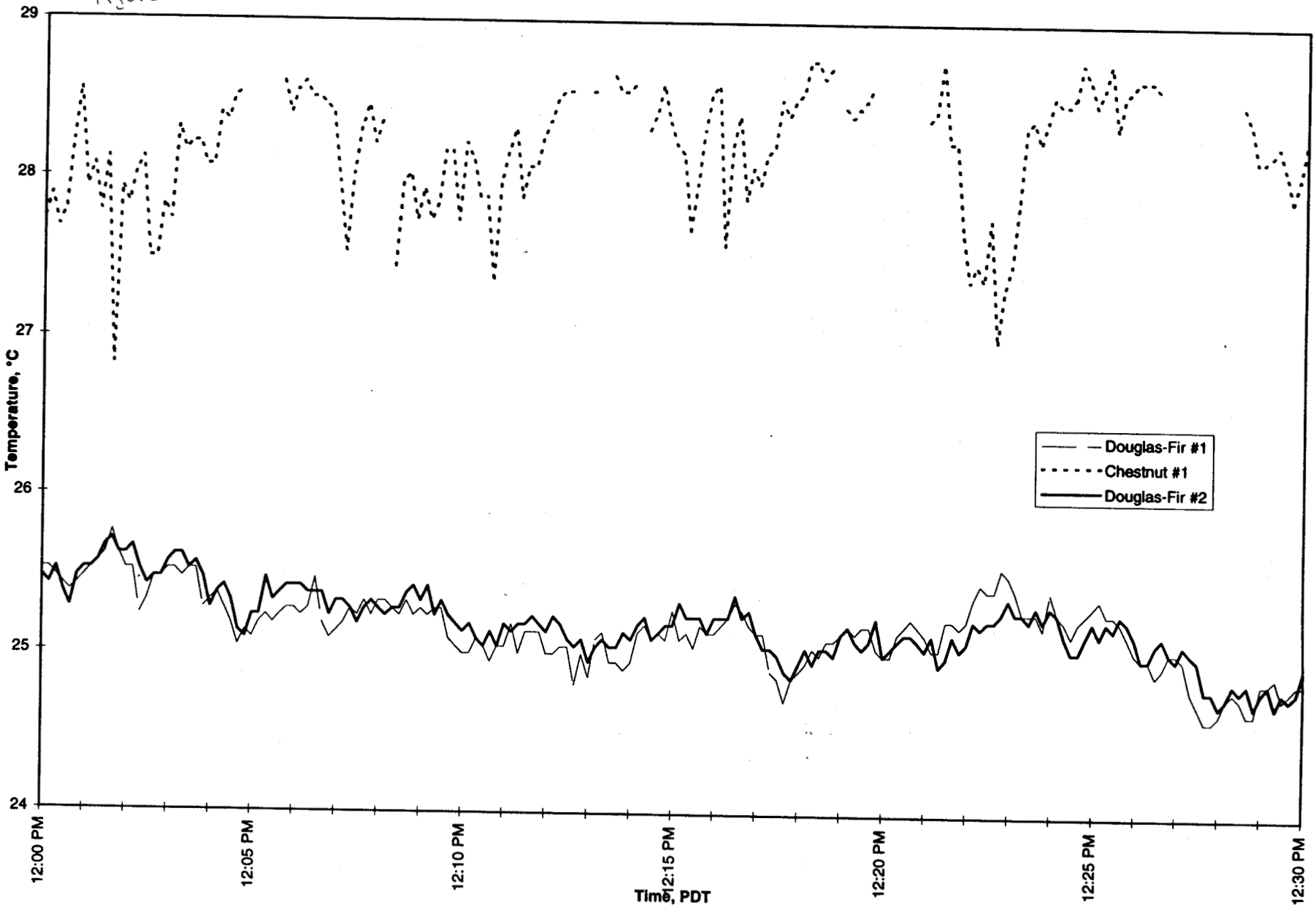
29
28
27
26
25
24
Temperature, °C
Douglas-Fir #1
Chestnut #1
Douglas-Fir #2
12:00 PM
12:05 PM
12:10 PM
12:15 PM
12:20 PM
12:25 PM
12:30 PM
Time, PDT

Figure 26

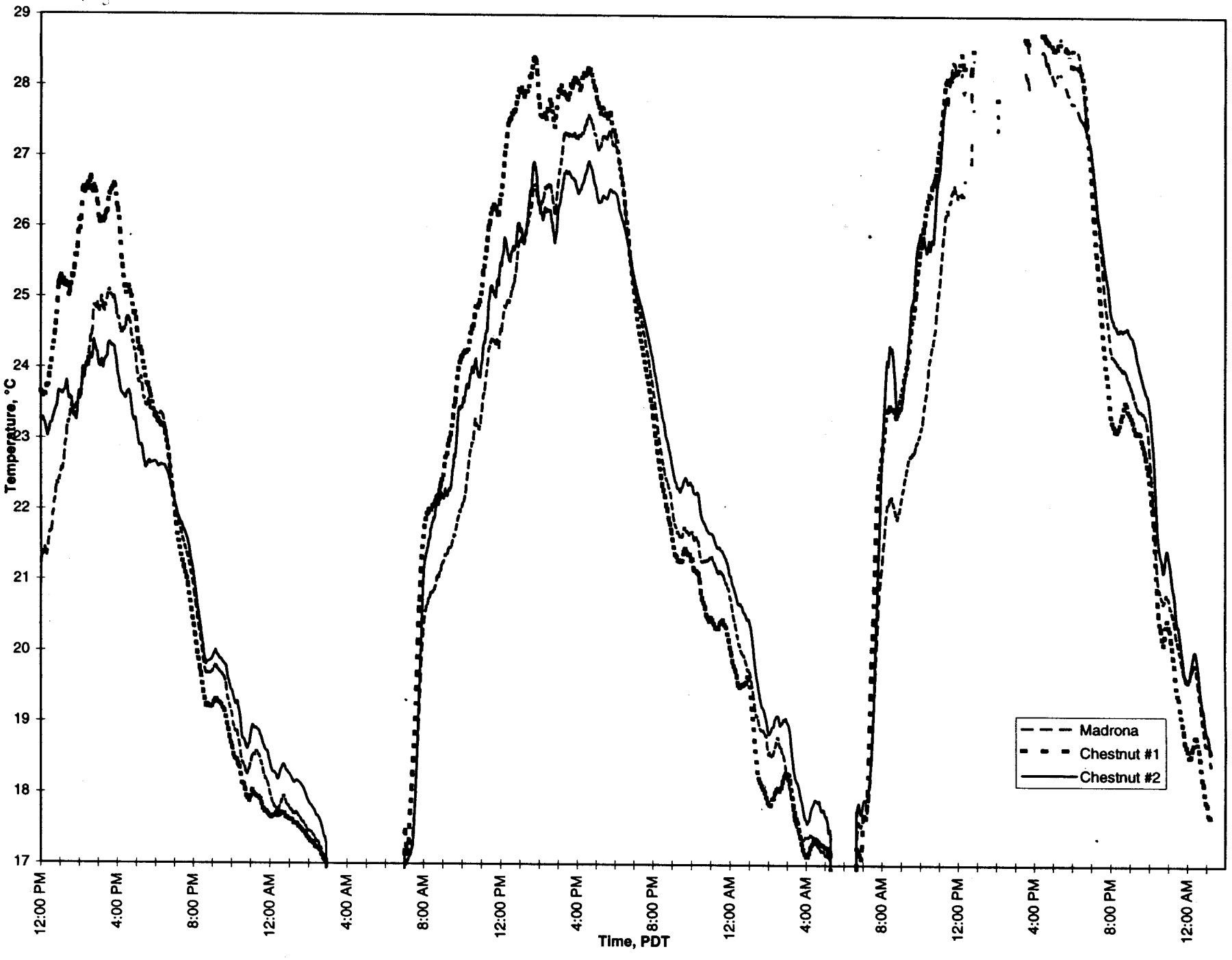
Temperature, °C
29
28
27
26
25
24
23
22
21
20
19
18
17
12:00 PM
4:00 PM
8:00 PM
12:00 AM
4:00 AM
8:00 AM
12:00 PM
4:00 PM
8:00 PM
12:00 AM
4:00 AM
8:00 AM
12:00 PM
4:00 PM
8:00 PM
12:00 AM
Time, PDT
Madrona
Chestnut #1
Chestnut #2

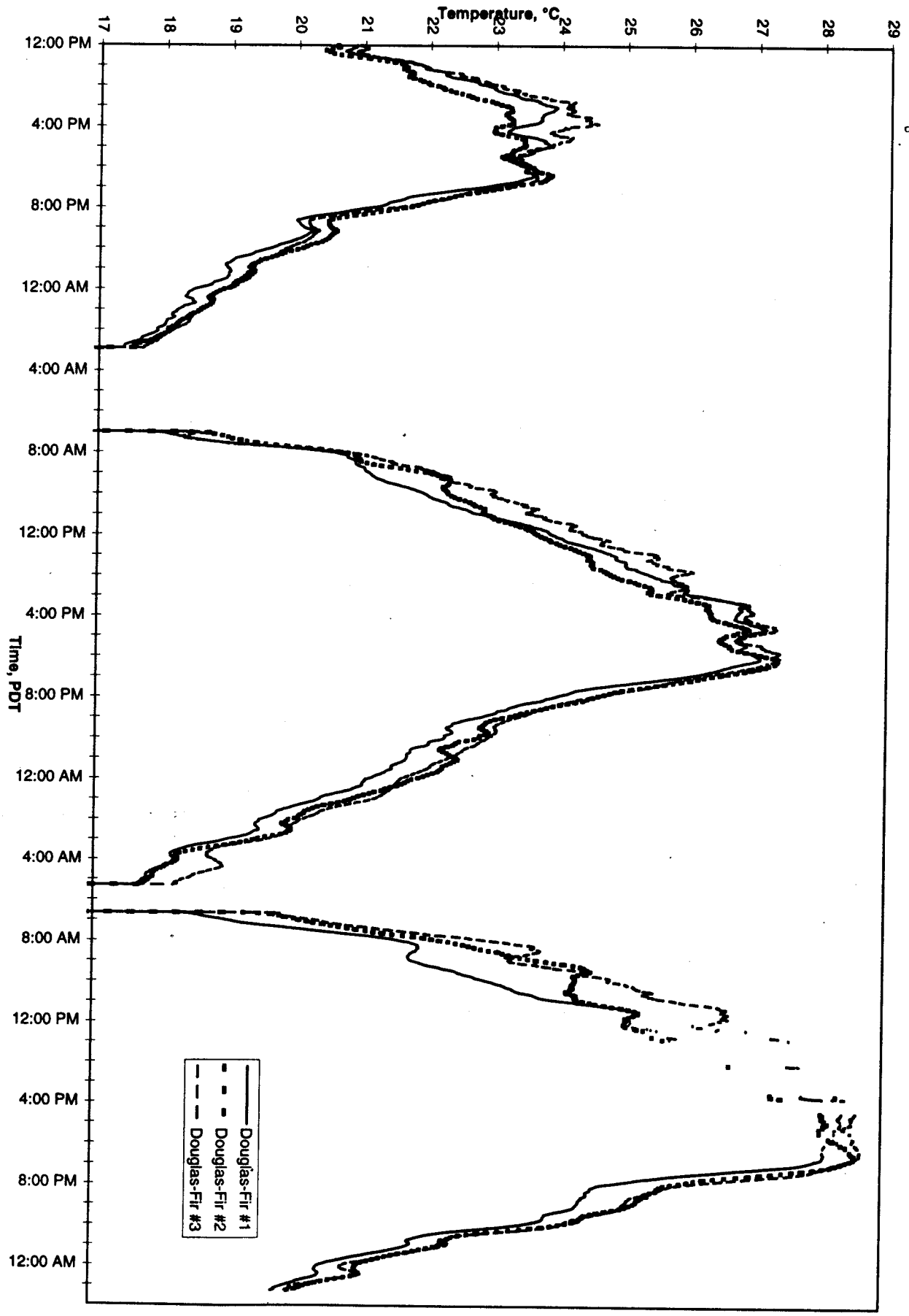
Temperature, °C
17
18
19
20
21
22
23
24
25
26
27
28
29
Time, PDT
12:00 PM
4:00 PM
8:00 PM
12:00 AM
4:00 AM
8:00 AM
12:00 PM
4:00 PM
8:00 PM
12:00 AM
4:00 AM
8:00 AM
12:00 PM
4:00 PM
8:00 PM
12:00 AM
Douglas-Fir #1
Douglas-Fir #2
Douglas-Fir #3

Figure 2C

Figure 2d

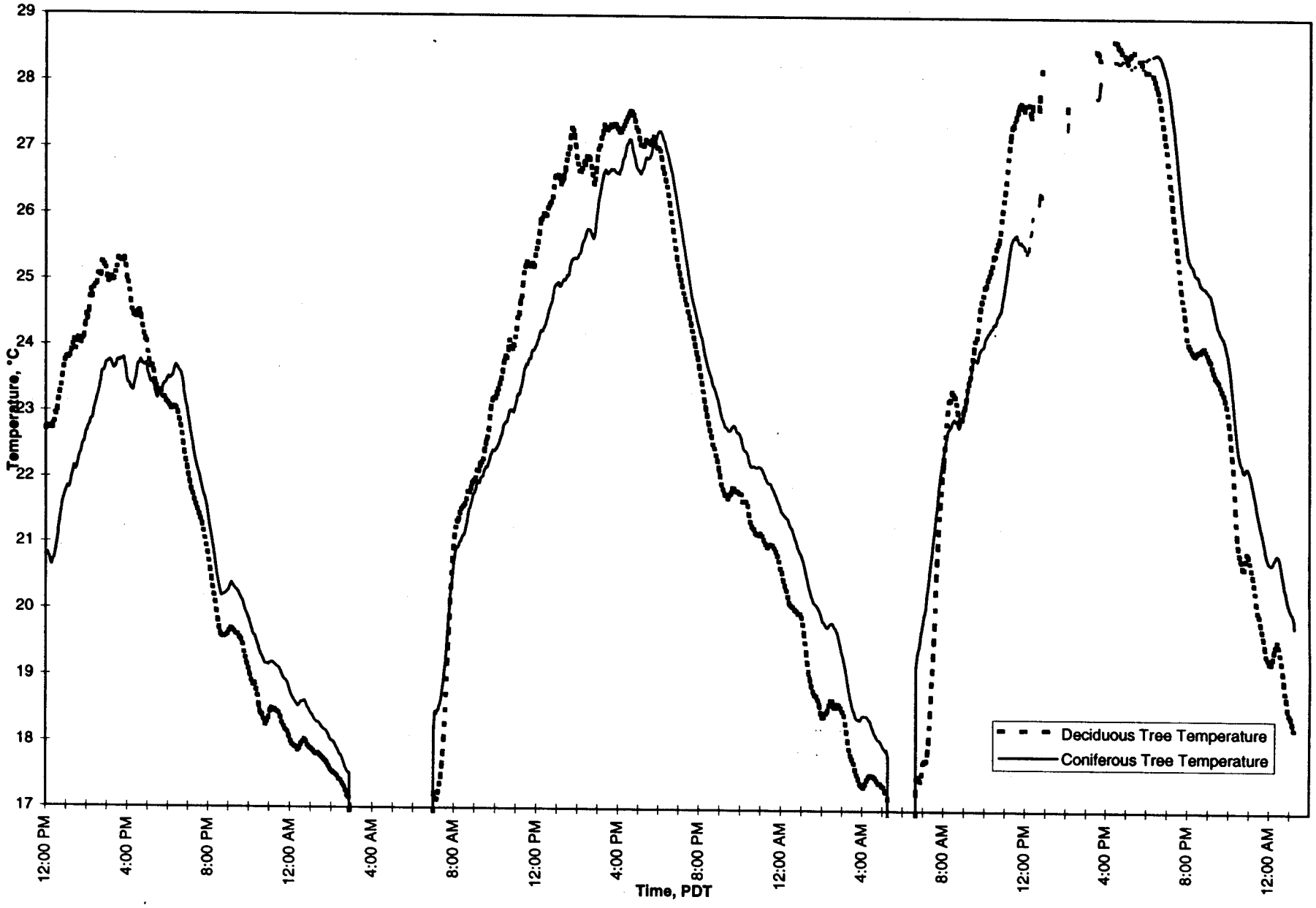
Temperature, °C
29
28
27
26
25
24
23
22
21
20
19
18
17
12:00 PM
4:00 PM
8:00 PM
12:00 AM
4:00 AM
8:00 AM
12:00 PM
4:00 PM
8:00 PM
12:00 AM
4:00 AM
8:00 AM
12:00 PM
4:00 PM
8:00 PM
12:00 AM
Time, PDT
Deciduous Tree Temperature
Coniferous Tree Temperature

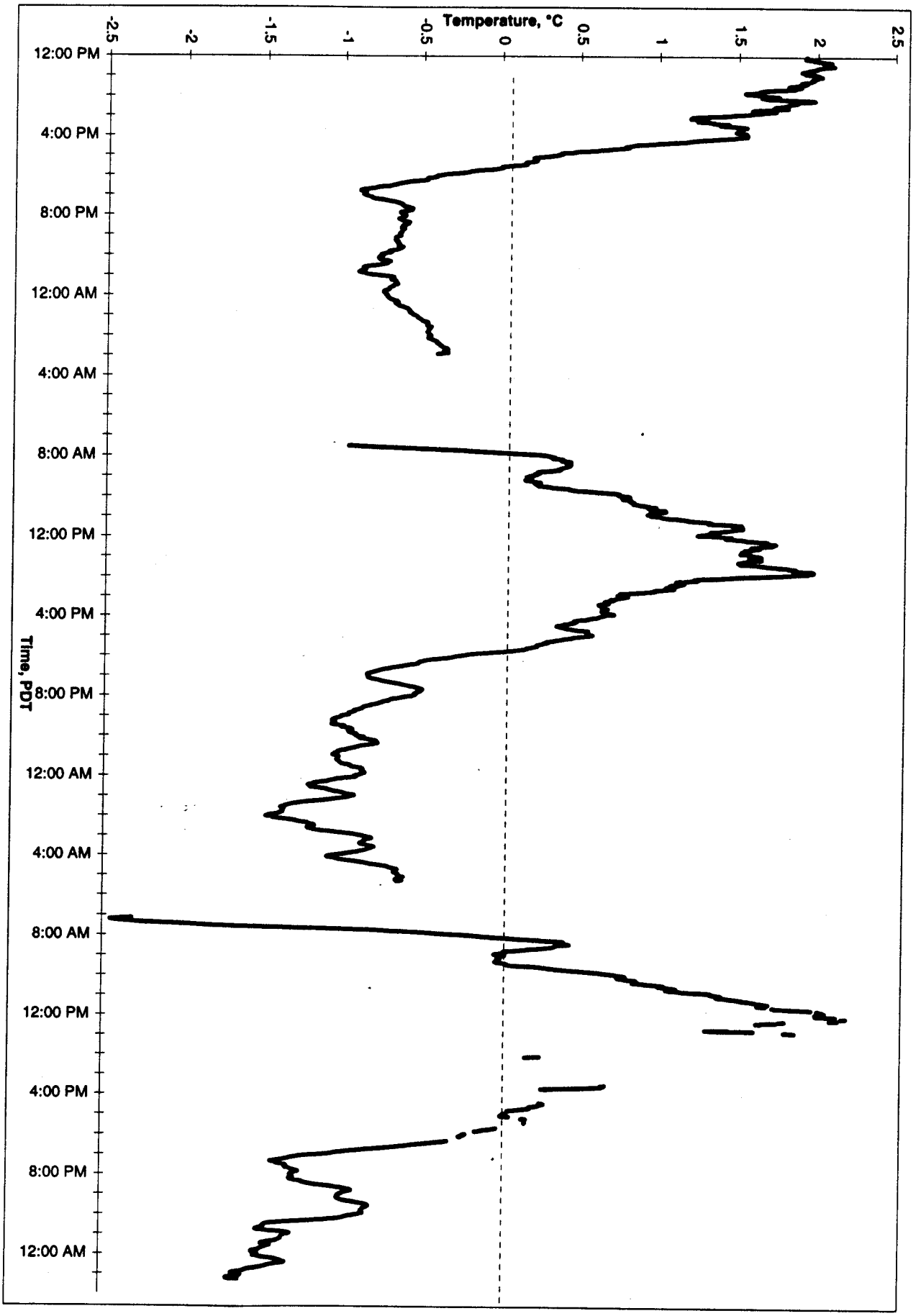
Temperature, °C
-2.5
-2
-1.5
-1
-0.5
0
0.5
1
1.5
2
2.5
Time, PDT
12:00 PM
4:00 PM
8:00 PM
12:00 AM
4:00 AM
8:00 AM
12:00 PM
4:00 PM
8:00 PM
12:00 AM
4:00 AM
8:00 AM
12:00 PM
4:00 PM
8:00 PM
12:00 AM

Figure 3

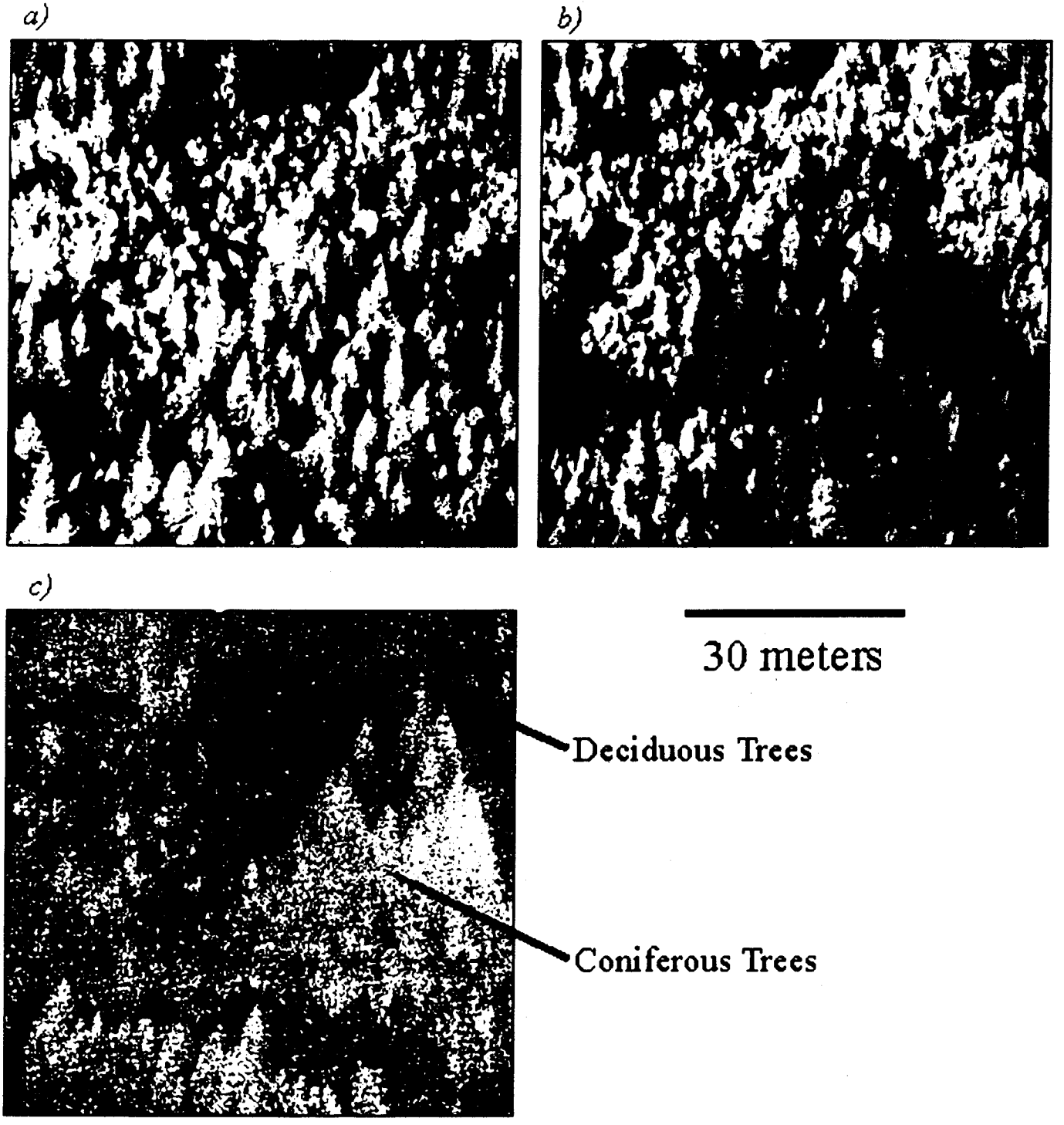

Figure 4: QWIP thermal images of a mixed coniferous/deciduous hillside: a) 7:00am, temperature range = 12-20°C, b) 2:00pm, temperature range = 20-30°C, c) 2:00am, temperature range = 10-15°C

Figure 5: False-color time-series "chronochrome". Red channel = 7:00am, green channel = 2:00pm, blue channel = 2:00am. Coniferous trees appear magenta and deciduous trees appear greenish.

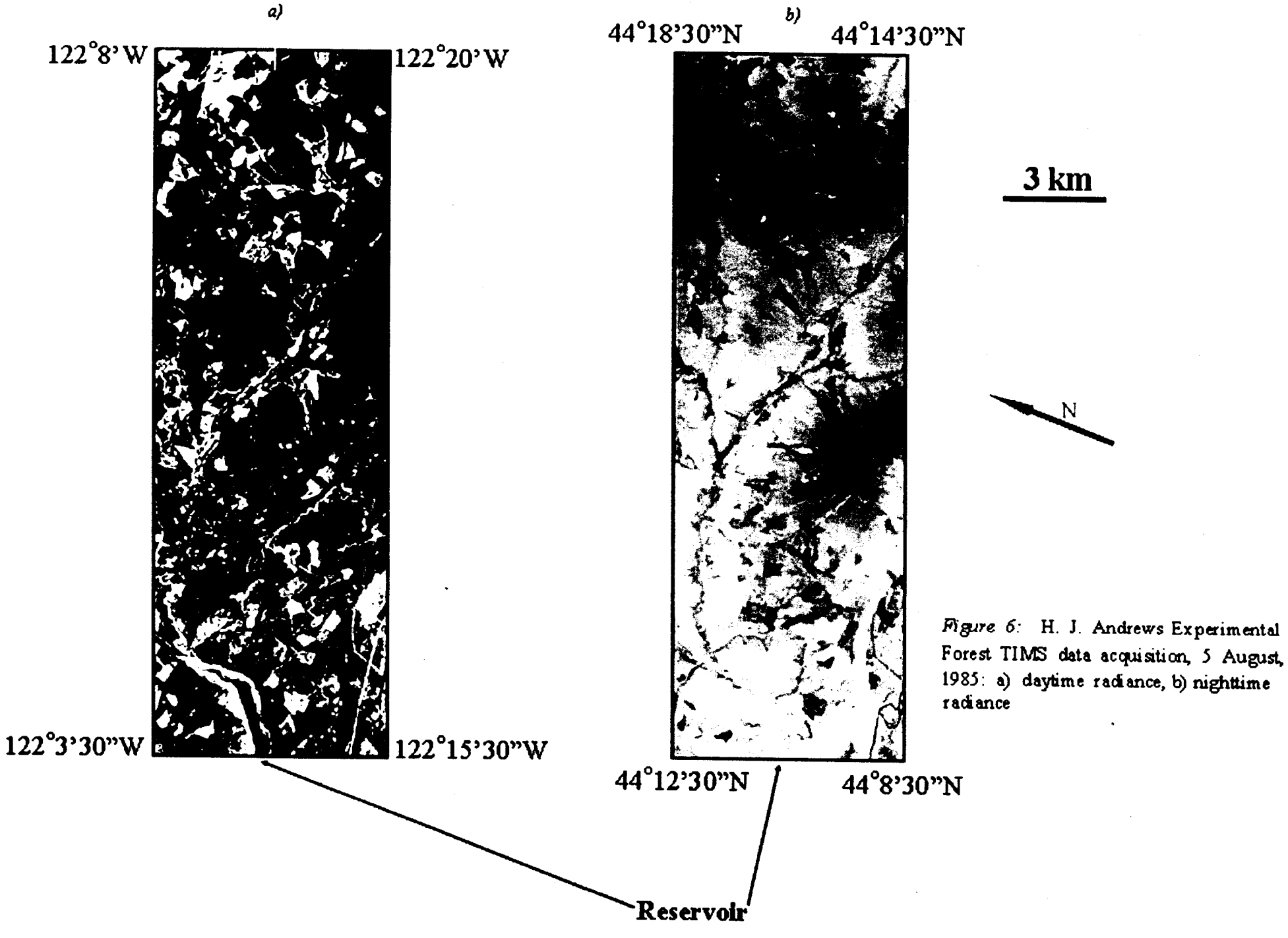

Figure 6: H. J. Andrews Experimental Forest TIMS data acquisition, 5 August, 1985: a) daytime radiance, b) nighttime radiance

Figure 7. Day/night ΔT image. Note: white pixels found in reservoir are due to out-of-range saturated pixels

Fig 5

a)

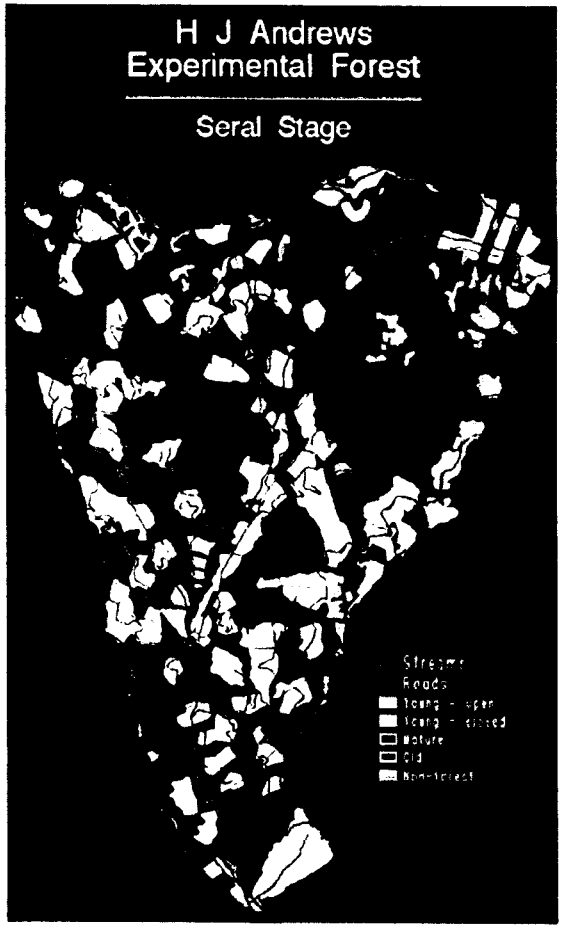

b)

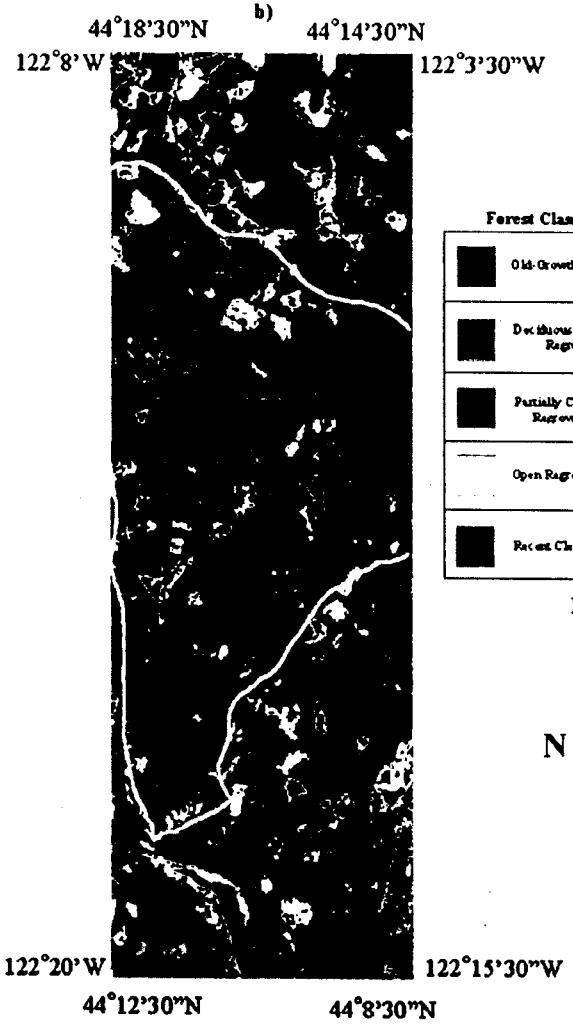

Explanation

Forest Class	Day/Night ΔT	ETI Value
Old-Growth	0.0 - 5.0°C	< 0.2
Deciduous Trees/Old Regrowth	5.1 - 10°C	0.196 - 0.1
Partially Closed Regrowth	10.1 - 15°C	0.099 - 0.067
Open Regrowth	15.1 - 25°C	0.066 - 0.04
Recent Clearcuts	> 25°C	> 0.04

Note: Water is Classified as Blue

3 km

N

Figure 5: Forest classification using effective thermal inertia derived from TIMS data, Willamette National Forest, Oregon. a) GIS ground-truth data, b) TIMS classification using ETI algorithm

FIGURE 9: Examples of coniferous and deciduous canopy structures (schematic)